Acta Cryst. (1996). B52, 519–534

Electron Density Study of a New Non-linear Optical Material: L-Arginine Phosphate Monohydrate (LAP). Comparison Between *X–X* and *X–(X + N)* Refinements

E. ESPINOSA,[a,b] C. LECOMTE,[a]* E. MOLINS,[b] S. VEINTEMILLAS,[b] A. COUSSON[c] AND W. PAULUS[c]

[a]*Laboratoire de Cristallographie et Modelisation des Materiaux Mineraux et Biologiques, LCM³B, URA CNRS No. 809, Faculté des Sciences, Université Henri Poincaré, Nancy 1, BP 239, 54506 Vandoeuvre-lés-Nancy CEDEX, France,* [b]*Institut de Ciència de Materials de Barcelona (CSIC), Campus de la UAB, 08193 Bellaterra, Barcelona, Spain, and* [c]*Laboratoire Léon Brillouin, CEA-CNRS, Saclay, France*

(*Received 20 July 1995; accepted 6 November 1995*)

Abstract

The crystal structure, thermal vibrations and electron density of L-arginine phosphate monohydrate (formally $C_6H_{15}N_4O_2^+.H_2PO_4^-.H_2O$) have been analysed using 130 K single-crystal X-ray diffraction data to a resolution of $(\sin\theta/\lambda)_{max} = 1.20\ \text{Å}^{-1}$. A multipolar pseudo-atom density model was fitted against the 6805 observed data with $I > 3\sigma(I)$, $[R(F) = 0.016, R_w(F) = 0.014, S = 1.39]$ in order to map the static valence-electron density distribution. Positional and thermal vibration parameters for H atoms were taken from neutron diffraction results. A comparison between the electron density $\rho(\mathbf{r})$, $\nabla^2\rho(\mathbf{r})$ and the electrostatic potential calculated from *X–X* and *X–(X + N)* refinements shows that reliable results may be obtained from *X–X* data only.

1. Introduction

L-Arginine phosphate monohydrate (LAP), $C_6H_{15}N_4O_2^+.H_2PO_4^-.H_2O$, is a non-linear organic crystal, whose properties were first reported by Xu, Tiang & Tan (1983). Because of its non-linear optical properties, LAP continues to be the subject of an increasing number of investigations, especially from the point of view of non-linear optical applications such as frequency conversion for high-power lasers (Eimerl *et al.*, 1989; Sasaki, Yokotani, Fujioka, Yamanaka & Nakai, 1989; Kitaoka, Yokotani & Sasaki, 1989). The prominent features of the present material are its high damage threshold, large non-linearity (Fuchs, Syn & Velsko, 1989; Yokotani, Sasaki, Yoshuda & Nakai, 1989) and the ease to grow large crystals of high optical quality (Espinosa *et al.*, 1994).

Experimental spectroscopic studies and thermal and electric properties of LAP have been studied (Dhanaraj, Srinivasan, Bhat, Jayanna & Subramanyam, 1992; Dhanaraj, Srinivasan & Bhat, 1991). Polarized Raman spectra of LAP single crystals have been studied at room temperature from 10 to 4000 cm^{-1}, together with the IR transmission spectrum of powder between 400 and 4000 cm^{-1} by Dhanaraj, Srinivasan & Bhat (1991). Recently, we have analysed the polarized far-IR reflectivity spectra of an LAP single crystal from 10 to 600 cm^{-1} and in the temperature range 7–250 K for both polarizations parallel and perpendicular to the twofold *b* axis (Espinosa *et al.*, 1994). The phonon modes were classified within their symmetry species and their frequencies and oscillator strength were calculated from the analysis of the experimental spectra.

The crystal structure of LAP at room temperature was first solved by Aoki, Nagano & Iitaka (1971) $[R(F) = 0.095, N_{obs} = 1229]$ and later the structure accuracy was significantly improved by Saenger & Wagner (1972) $[R(F) = 0.035, N_{obs} = 1396]$.

The present paper is devoted to the comparison between *X–X* and *X–(X + N)* electron density and the related properties (net charges, dipole moment, electrostatic potential and topology of the electron density) in LAP. Both a detailed analysis of the intermolecular interactions in LAP crystals and a comparative study between *ab initio* SCF theoretical calculations and the *X–(X + N)* model (described below) are in progress and will be published elsewhere.

2. Experimental

2.1. *Crystal growth*

LAP single crystals were grown from a supersaturated aqueous solution, by slow evaporation at 323 K. A subsaturated solution of LAP was prepared by adding orthophosphoric acid (49.63 g 85%, Merck AR) to a stirred suspension of L-arginine (75 g, Carlo Erba RPE) in 500 cm^3 of distilled water at room temperature. This solution was placed in a 1 l crystallizator sitting in a 9 l desiccator partially submerged in a thermostatic bath kept at the desired growth temperature. Evaporation occurs by condensation of water on the relatively cool desiccator lid. Under the above-mentioned conditions, the rate of solvent extraction was 37 g H_2O/day; a typical experiment lasts 7 days. The volumes of the thick (100) plate-like crystals obtained range between 1 mm^3 and 3 cm^3.

2.2. *Crystal data*

$C_6H_{15}N_4O_2^+.H_2PO_4^-.H_2O$, M_r = 290.22, monoclinic, $P2_1$, Z = 2, ρ_{calc} = 1.54 g cm^{-3}, T = 130 K; X-ray lattice parameters: a = 7.319 (1), b = 7.912 (2), c = 10.779 (3) Å, β = 98.05 (2)°, V = 618.0 Å^3; neutron lattice parameters: a = 7.333 (6), b = 7.93 (2), c = 10.81 (2) Å, β = 98.0 (1)°, V = 622.5 Å^3.

2.3. *X-ray data collection*

A colourless transparent prismatic single crystal of dimensions 0.22 × 0.26 × 0.32 mm^3 was used for the X-ray diffraction experiments at T = 130 ± 3 K. The X-ray source was graphite-monochromated Mo $K\alpha$ radiation (μ_{calc} = 0.24 mm^{-1}) from a sealed tube. Measurements were made on an Enraf–Nonius CAD-4 diffractometer, equipped with a nitrogen jet stream low-temperature system (Soterem N-jet) installed in a drybox to prevent ice formation on the crystal; the gas stream temperature was monitored to 110 ± 3 K at the nozzel, corresponding to a temperature of the crystal of 130 K, as calibrated using the paraferroelectric KDP transition (123 K).

Lattice parameters were obtained by least-squares fit to the optimized setting angles of 25 reflections with $26 < 2\theta < 56°$. Intensity data were recorded as ω–2θ scan profiles to a resolution $(\sin\theta/\lambda)_{max} \leq 1.20$ Å^{-1} for a total of 15 513 reflections ($-17 \leq h \leq 17$, $-18 \leq k \leq 18$, $-25 \leq l \leq 0$) in the following way: for $\sin\theta/\lambda \leq 1.05$ Å^{-1} all the reflections in one hemisphere were collected; after a conventional refinement against these data, higher-order intensities were calculated to $\sin\theta/\lambda$ = 1.20 Å^{-1} and only reflections with an estimated $I > 5\sigma(I)$ were collected in the hemisphere. All reflections were collected at ψ = 0°. During the data collection five standard reflections, $(1\bar{4}1)$, $(\bar{2}13)$, $(14\bar{3})$, $(\bar{3}41)$ and $(\bar{2}\bar{1}\bar{3})$, were measured at 3 h intervals. The total scan width ($\Delta\omega$) was 1.05 + 0.35 tgθ, with a fixed horizontal and vertical detector aperture of 4 × 6 mm^2. A prescan speed v = dω/dt of 2.75° min^{-1} and a final scan speed depending of the signal-to-noise ratio ($0.75 < v < 2.75°$ min^{-1}) were used for the low-angle data collection ($\sin\theta/\lambda \leq 1.05$ Å^{-1}). The high-order data were measured at a constant scan speed data (0.5° min^{-1}). The total exposure time was 517 h and the total experiment time was 29 days for a total of 15 513 collected reflections. No diffractometer or temperature problem occurred during the experiment.

2.4. *Neutron data collection*

A transparent prismatic single crystal of 3.5 × 2.5 × 3.0 mm^3 was used to measure the 130 K neutron diffraction data (μ_{exp} = 0.22 mm^{-1}). The measurements were performed at the Léon–Brillouin Laboratory (CNRS–CEA, Saclay, France), with a Stoe four-circle diffractometer on the 5C2 channel, which is at the end of a neutron hot source line [λ = 0.8302 (2) Å] at the ORPHEE reactor. The diffractometer was equipped with a Cu (220) monochromator (which has also an erbium filter) and a nitrogen vapour stream low-temperature cryostat. The crystal temperature was maintained at 130 ± 5 K. Lattice parameters were obtained by least-squares fit to the setting angles of 16 reflections with $21.2 < 2\theta < 32.4°$. The latter values were not optimized. Intensity data were recorded as ω scan profiles up to a resolution of $(\sin\theta/\lambda)_{max} < 0.79$ Å^{-1} (two sets of equivalent reflections were measured for data with $\sin\theta/\lambda < 0.5$ Å^{-1}) for a total of 4139 reflections ($-12 \leq h \leq 0$, $-13 \leq k \leq 13$, $-17 \leq l \leq 17$). During the data collection two standard reflections, (020) and (210), were measured at 450 min intervals.

2.5. *X-ray data processing*

Data reduction and error analysis were performed using the *DREAR* programs (Blessing, 1987, 1989). Reflection integration limits were taken from a Lorentzian model of the peak-width variations. A polynomial fit to the decay of the standard reflection intensities (~3%), over the 517 h X-ray exposure time, was applied to scale the data and derive the instrumental instability coefficient ($<p>$ = 0.8%) used in the calculation of $\sigma^2(|F|^2) = \sigma_c^2(|F|^2) + (<p>|F|^2)^2$. The 15 513 data with $\sin\theta/\lambda \leq 1.20$ Å^{-1} were first averaged with the $2/m$ symmetry to give 7203 unique data ($I > 0$), of which 6465 have $I > 3\sigma(I)$. Internal agreement factors were $R_{int}(F^2)$ = 0.015 and $R_w(F^2)$ = 0.029 for all data. Later, in order to correct anomalous dispersion effects, the data set was averaged according to 2 symmetry to give 13 589 unique data ($I > 0$), of which 12 697 have $I > 3\sigma(I)$; internal agreement factors were $R_{int}(F^2)$ = 0.010 and $R_w(F^2)$ = 0.013 for all data (685 multiple measurements). Several attempts to correct for absorption effects led to equal or slightly worse R_{int} values, therefore, no correction was finally applied ($\mu R_{max} < 0.1$).

2.6. *Neutron data processing*

Over the 288 h neutron exposure time, no decay was detected in the standard reflections intensities ($\Delta I/I < 0.5\%$). Data were corrected for Lorentz effects and absorption [Gaussian integration method, crystal faces morphology: (001), $(\bar{1}0\bar{1})$, (110), (001), (101), $(00\bar{1})$, $(1\bar{1}0)$, $(\bar{1}10)$ and (102); $0.56 < T < 0.61$]. Data averaging was not carried out because of possible anisotropic extinction effects. Of the 4139 measured reflections, 3176 were considered to be observed [$I > 3\sigma(I)$].

3. Initial X-ray least-squares refinements

3.1. *High-order refinement*

High-order (HO) refinement was performed against the low-temperature $2/m$ averaged data, using 1660 reflections with $1.0 < \sin\theta/\lambda < 1.2$ Å^{-1} and $I > 2\sigma(I)$.

Table 1. *Statistical indices as a function of the scale factor for HO refinements (162 parameters)*

Indices are defined as: $\chi^2 = \Sigma w\Delta^2$, where $\Delta = F_o - (k^{-1}y^{1/2}F_c)$ and $w = 1\sigma^2(F_o)$ (the extinction parameter y was not refined at this level), $R = \Sigma\Delta/\Sigma F_o$, $R_w = (\chi^2/\Sigma wF_o^2)^{1/2}$ and $S = [\chi^2/(N_{obs} - N_{par})]^{1/2}$, where N_{obs} and N_{par} are the number of observables and the number of refined parameters, respectively.

k^{-1}	1.30	1.29	1.28	1.27	1.26	1.25	1.22	1.18
R	0.0338	0.0338	0.0338	0.0338	0.0339	0.0339	0.0341	0.0347
R_w	0.0324	0.0324	0.0324	0.0324	0.0324	0.0324	0.0326	0.0331
S	1.04	1.04	1.04	1.04	1.04	1.04	1.05	1.06
$\Sigma w\Delta^2$	1622.7	1618.7	1616.4	1615.7	1616.7	1619.5	1638.6	1691.2

We found the scale factor very badly determined due to very high correlation with the overall temperature factor: eight least-squares refinements were therefore performed with the same data set at fixed scale factors ($1.18 < k^{-1} < 1.30$) for anisotropic non-H atoms. These refinements led to the same statistical indices, whatever the choice of k^{-1} (see Table 1).

Therefore, the scale cannot be unambiguously determined due to the correlation between k^{-1} and U parameters. We chose the scale factor value at the minimum value of $\Sigma w\Delta^2$ ($k^{-1} = 1.27$). This value differs from the scale factor found for all data refinement by 2%.

3.2. *Absolute configuration and anomalous dispersion correction*

Because of the anomalous dispersion of the P atom [$f' = 0.090$ and $f'' = 0.095$ (Cromer, 1974)], the Friedel pairs are not strictly equivalent. Thus, with a data set averaged over 2 Laue symmetry, it is possible to determine the absolute configuration. The scale factor and the anisotropic thermal vibrations for the non-H atoms (for two sets of positional parameters: xyz and $x\bar{y}z$) were refined with a spherical atoms model. Refinements were performed with HO data ($1.0 < \sin\theta/\lambda < 1.2$ Å^{-1}) and all data ($0 < \sin\theta/\lambda < 1.2$ Å^{-1}). As expected, the agreement statistics given in Table 2 confirm the L-configuration of the arginine cation. Then, in order to remove anomalous dispersion effects, a first multipolar refinement was performed using the Hansen–Coppens model (Hansen & Coppens, 1978) with the 2 symmetry averaged data [$N_{obs} = 12697$, $I > 3\sigma(I)$]. In this model the atomic electron density is described by

$$\rho_{at}(\mathbf{r}) = \rho_c(r) + P_v\kappa^3\rho(\kappa r) + \sum_{l=0}^{l_{max}}\sum_{m=0}^{l}\kappa'^3 R_{nl}(\kappa' r)P_{lm\pm}y_{lm\pm}(\theta,\varphi), \quad (1)$$

where ρ_c and ρ_v are spherically averaged Hartree–Fock core and valence densities, $y_{lm\pm}$ are multipolar spherical harmonic angular functions in real form, $R_{nl}(\kappa' r)$ are Slater-type radial functions, κ and κ' are the expansion–contraction parameters and P_v and $P_{lm\pm}$ the population parameters. The n_l and ζ parameters used for H, C, N and O atoms were 1 and 2.26; 2, 2, 3 and 3.0; 2, 2, 3 and 3.8; 2, 2, 3 and 4.5 bohr^{-1}, respectively. The choice of the n_l and ζ parameters for P (6, 6, 6, 6 and 3.6 bohr^{-1}) and O(P) (1, 2, 4 and 4.5 bohr^{-1}) atoms was deduced from an analysis of the residual electron density (Espinosa, 1994) calculated from a multipolar refinement of theoretical H_3PO_4 structure factors (Moss & Blessing, 1984; Moss, 1983). Fig. 1 shows the local axis scheme used in the asymmetric unit. Four types of H atoms were defined [H(C), H(N), H(Ow), H(O(P))] and chemically equivalent O and N atoms were constrained to have the same multipole parameters (O1 = O2, O3 = O4, O5 = O6 and N3 = N4). Symmetry m for O5, O6, N3, N4, C1 and C6 atoms was also imposed. The thermal and positional parameters obtained from the L-configuration HO refinement, the scale factors from all data, were used as starting

Table 2. *Statistical results for* L- *and* D*-configurations of arginine cation with a spherical atoms model [HO data ($1 < \sin\theta/\lambda < 1.2$ Å^{-1}) and all data ($0 < \sin\theta/\lambda < 1.2$ Å^{-1})] and final agreement factors for X–(X+N) and X–X multipolar and κ refinement models ($0 < \sin\theta/\lambda < 1.2$ Å^{-1})*

HO	R	R_w	S	N_{obs}	k^{-1}
L-configuration	0.040	0.043	1.36	3099	1.270 (10)
D-configuration	0.042	0.045	1.44	3099	1.271 (11)
All data					
L-configuration	0.028	0.032	2.64	12697	1.2482 (6)
D-configuration	0.030	0.034	2.79	12697	1.2481 (7)
Multipolar refinement					
X–(X + N)	0.016	0.014	1.39	6805	1.0007 (2)
X–X	0.017	0.016	1.51	6805	1.0006 (2)
κ refinement					
X–(X + N)	0.023	0.027	2.53	6805	1.0007 (-)
X–X	0.024	0.029	2.63	6805	1.0006 (-)

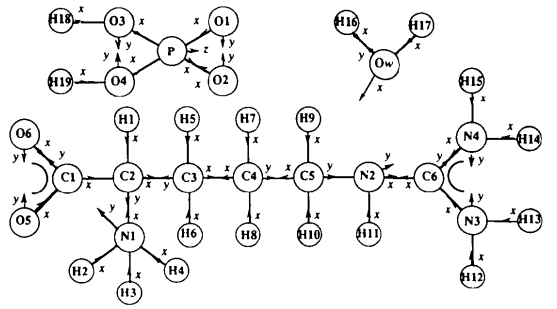

Fig. 1. Local Cartesian axis for the atom-centred multipole functions (*MOLLY* definition) in the asymmetric unit of LAP.

parameters. H atoms were found by difference-Fourier syntheses ($\sin\theta/\lambda<0.5$ Å^{-1}) and refined isotropically. Their coordinates were then shifted by extending along the Csp^3—H, N—H, O(P)—H and Ow—H bond vectors to average bond distance values from neutron diffraction [1.085, 1.032, 0.995 and 0.970 Å, respectively (Kvick, Koetzle & Thomas, 1974; Allen, 1986; Blessing, 1988)]. These distances were kept fixed during all further refinements. The core and radial valence scattering factors $<j_0>$ for the non-H atoms were calculated from Clementi wavefunctions (Clementi, 1965) and a bound atom form factor for hydrogen (Stewart, Davidson & Simpson, 1965) was used by imposing a starting κ value of 1.16 to the scattering factor of the free H atom. The real and imaginary dispersion corrections to the form factors given by Cromer (1974) were used in the structure factor calculations. At the end of this refinement the observed structure factors (put at the absolute scale) were corrected from the anomalous dispersion effect (Souhassou, Espinosa, Lecomte & Blessing, 1995) by

$$A^o_{obs} = F^a_{obs}A^a_{calc}/F^a_{calc} - (A^a_{calc} - A^o_{calc})$$
$$B^o_{obs} = F^a_{obs}B^a_{calc}/F^a_{calc} - (B^a_{calc} - B^o_{calc}),$$

where A and B are the real and imaginary parts of the complex structure factors and the upper o and a denote the corrected and uncorrected anomalous dispersion effects, respectively. This correction allows to average the observed structure factors according to point group $2/m$. This correction improved slightly the internal agreement factors [$R_{int}(F^2)$ = 0.013 and $R_{w=1}(F^2)$ = 0.025] for the 6805 unique reflections (0.015 and 0.029, respectively, for 7203 unique reflections before correction of anomalous dispersion effects).

Finally, this data set was used to study the electron density of LAP in the X–X and X–(X + N) refinements.

4. Neutron least-squares refinement

Crystal structure was refined against neutron data using a modified version of the *MOLLY* program (Hansen & Coppens, 1978) and the neutron form factors from Sears (1992). H atoms were refined with anisotropic thermal parameters. The refinement was against F [w = $1/\sigma^2(F)$]. At the end of the refinement, statistical factors were R = 0.039, R_w = 0.041, S = 2.38 for N_{obs} = 3176 observed reflections [$I > 3\sigma(I)$] and N_{par} = 339 parameters (N_{obs}/N_{par} = 9.4). Because of the severe anisotropic extinction, the Becker–Coppens extinction correction (Becker & Coppens, 1974; Lorentz type I), with a Thornley–Nelmes g tensor model (Thornley & Nelmes, 1974), was applied. At the end of the convergence, the g tensor values (in rad^2) were g_{11} = 158 (9) × 10^{-8}, g_{22} = 196 (11) × 10^{-8}, g_{33} = 11.6 (3) × 10^{-8}, g_{12} = 3 (5) × 10^{-8}, g_{13} = 24 (1) × 10^{-8} and g_{23} =

Table 3. *Bond distances (Å) and angles (°) from: (a) neutron, (b) X-X and (c) X-(X + N) models*

P—O1	1.510 (3)	C4—H7	1.100 (4)
	1.5072 (4)		1.085 (-)
	1.5062 (5)		1.107 (-)
P—O2	1.500 (3)	C4—H8	1.101 (4)
	1.4981 (4)		1.085 (-)
	1.4981 (4)		1.108 (-)
P—O3	1.598 (3)	C5—H9	1.088 (4)
	1.5911 (5)		1.085 (-)
	1.5901 (5)		1.086 (-)
P—O4	1.571 (3)	C5—H10	1.103 (4)
	1.5676 (5)		1.085 (-)
	1.5673 (5)		1.117 (-)
O5—C1	1.234 (3)	N2—H11	1.023 (4)
	1.2450 (5)		1.032 (-)
	1.2454 (5)		1.026 (-)
O6—C1	1.278 (3)	N3—H12	1.019 (4)
	1.2690 (5)		1.032 (-)
	1.2687 (5)		1.022 (-)
N1—C2	1.497 (2)	N3—H13	1.015 (4)
	1.4895 (5)		1.032 (-)
	1.4886 (5)		1.009 (-)
N2—C5	1.465 (2)	N4—H14	1.010 (4)
	1.4584 (6)		1.032 (-)
	1.4582 (5)		1.014 (-)
N2—C6	1.329 (2)	N4—H15	1.030 (4)
	1.3310 (5)		1.032 (-)
	1.3312 (5)		1.021 (-)
N3—C6	1.344 (2)	Ow-H16	0.968 (5)
	1.3387 (5)		0.970 (-)
	1.3392 (5)		0.967 (-)
N4-C6	1.330 (2)	Ow—H17	0.983 (5)
	1.3289 (5)		0.970 (-)
	1.3283 (5)		0.992 (-)
C1—C2	1.541 (2)	O3—H18	1.011 (4)
	1.5339 (5)		0.995 (-)
	1.5339 (5)		1.011 (-)
C2—C3	1.536 (2)	O4—H19	1.008 (4)
	1.5308 (6)		0.995 (-)
	1.5314 (5)		1.000 (-)
C3—C4	1.531 (2)		
	1.5248 (6)		
	1.5250 (5)		
C4—C5	1.529 (2)		
	1.5263 (6)		
	1.5262 (5)		
C2—H1	1.106 (4)		
	1.085 (-)		
	1.114 (-)		
N1—H2	1.039 (4)		
	1.032 (-)		
	1.046 (-)		
N1—H3	1.047 (4)		
	1.032 (-)		
	1.041 (-)		
N1—H4	1.053 (4)		
	1.032 (-)		
	1.049 (-)		
C3—H5	1.104 (4)		
	1.085 (-)		
	1.105 (-)		
C3—H6	1.098 (4)		
	1.085 (-)		
	1.089 (-)		
O1—P—O2	115.5 (2)	N1—C2—C1	109.7 (1)
	114.97 (3)		109.52 (3)
	114.95 (3)		109.54 (3)

Table 3 (*cont.*)

O1—P—O3	105.2 (2)	N1—C2—C3	109.1 (1)
	105.38 (3)		109.56 (3)
	105.39 (3)		109.56 (3)
O1—P—O4	111.0 (2)	N1—C2—H1	106.5 (2)
	111.55 (3)		105.8 (-)
	111.53 (3)		106.9 (-)
O2—P—O3	111.3 (2)	C1—C2—C3	111.7 (1)
	110.97 (3)		111.70 (3)
	110.96 (3)		111.67 (3)
O2—P—O4	107.2 (2)	C1—C2—H1	108.5 (2)
	107.44 (3)		110.0 (-)
	107.43 (3)		108.0 (-)
O3—P—O4	106.2 (2)	C3—C2—H1	111.1 (2)
	106.23 (4)		110.1 (-)
	106.27 (4)		111.1 (-)
P—O3—H18	117.0 (3)	C2—C3—C4	112.2 (1)
	119.8 (-)		112.71 (3)
	117.4 (-)		112.70 (3)
P—O4—H19	115.1 (2)	C2—C3—H5	109.9 (3)
	111.1 (-)		108.7 (-)
	114.7 (-)		109.6 (-)
H16—O*w*—H17	108.4 (4)	C2—C3—H6	107.3 (3)
	103.7 (-)		105.5 (-)
	107.6 (-)		107.2 (-)
C2—N1—H2	108.1 (2)	C4—C3—H5	110.7 (3)
	114.1 (-)		111.6 (-)
	107.9 (-)		110.1 (-)
C2—N1—H3	108.5 (2)	C4—C3—H6	108.6 (3)
	114.2 (-)		112.9 (-)
	108.3 (-)		108.5 (-)
C2—N1—H4	111.8 (2)	H5—C3—H6	108.1 (3)
	115.3 (-)		105.0 (-)
	111.6 (-)		108.6 (-)
H2—N1—H3	108.5 (3)	C3—C4—C5	112.3 (1)
	99.0 (-)		112.37 (3)
	108.4 (-)		112.34 (3)
H2—N1—H4	110.1 (3)	C3—C4—H7	110.4 (3)
	110.3 (-)		109.8 (-)
	109.9 (-)		110.8 (-)
H3—N1—H4	109.8 (3)	C3—C4—H8	109.9 (2)
	102.2 (-)		109.9 (-)
	110.6 (-)		110.0 (-)
C5—N2—C6	126.2 (1)	C5—C4—H7	108.1 (3)
	126.03 (4)		109.6 (-)
	126.02 (4)		108.5 (-)
C5—N2—H11	116.6 (2)	C5—C4—H8	108.6 (3)
	114.7 (-)		111.0 (-)
	116.3 (-)		108.6 (-)
C6—N2—H11	117.2 (2)	H7—C4—H8	107.3 (3)
	119.2 (-)		103.9 (-)
	117.6 (-)		106.4 (-)
C6—N3—H12	119.7 (3)	N2—C5—C4	111.0 (1)
	120.6 (-)		111.36 (3)
	119.6 (-)		111.38 (3)
C6—N3—H13	119.9 (3)	N2—C5—H9	109.4 (2)
	123.3 (-)		108.4 (-)
	119.8 (-)		110.2 (-)
H12—N3—H13	120.3 (4)	N2—C5—H10	108.3 (3)
	115.9 (-)		111.1 (-)
	120.5 (-)		108.4 (-)
C6—N4—H14	123.4 (2)	C4—C5—H9	110.3 (3)
	122.0 (-)		114.3 (-)
	123.2 (-)		110.3 (-)
C6—N4—H15	117.4 (3)	C4—C5—H10	110.0 (2)
	118.4 (-)		112.0 (-)
	117.2 (-)		109.6 (-)
H14—N4—H15	118.9 (3)	H9—C5—H10	107.8 (3)
	119.3 (-)		99.1 (-)
	119.2 (-)		106.9 (-)

Table 3 (*cont.*)

O5—C1—O6	125.6 (2)	N2—C6—N3	118.8 (1)
	125.58 (4)		118.68 (4)
	125.59 (4)		118.66 (4)
O5—C1—C2	118.5 (2)	N2—C6—N4	122.5 (1)
	118.07 (4)		122.33 (4)
	118.05 (3)		122.34 (3)
O6—C1—C2	115.9 (1)	N3—C6—N4	118.7 (1)
	116.33 (3)		118.99 (4)
	116.34 (3)		118.99 (4)

Table 4. *Intermolecular bond distances (Å) and angles (°) from: (a) neutron, (b) X-X and (c) X-(X+N) models*

	H···O (Å)	X···O (Å)	X—H···O (°)
O4—H19···O1^{ii}	1.569 (4)	2.568 (3)	169.9 (4)
	1.652 (-)	2.5588 (7)	149.4 (-)
	1.570 (-)	2.5604 (7)	169.7 (-)
O3—H18···O6^{iii}	1.592 (4)	2.598 (3)	173.0 (4)
	1.654 (-)	2.5933 (6)	155.8 (-)
	1.589 (-)	2.5939 (6)	172.5 (-)
N1—H4···O2^{i}	1.736 (4)	2.774 (2)	167.8 (3)
	1.744 (-)	2.7715 (6)	173.2 (-)
	1.739 (-)	2.7719 (6)	167.2 (-)
N1—H3···O2^{iii}	1.767 (4)	2.801 (2)	168.6 (3)
	1.807 (-)	2.7952 (6)	158.9 (-)
	1.767 (-)	2.7951 (6)	168.8 (-)
O*w*—H17···O5^{iv}	1.819 (4)	2.798 (3)	173.3 (4)
	1.828 (-)	2.7790 (7)	165.7 (-)
	1.793 (-)	2.7786 (6)	172.4 (-)
N1—H2···O1^{v}	1.827 (4)	2.829 (2)	160.8 (3)
	1.881 (-)	2.8238 (7)	150.3 (-)
	1.815 (-)	2.8244 (6)	161.2 (-)
N4—H15···O3^{ii}	1.829 (4)	2.852 (2)	171.9 (4)
	1.824 (-)	2.8450 (6)	169.4 (-)
	1.831 (-)	2.8455 (5)	171.9 (-)
O*w*—H16···O5^{vi}	1.846 (5)	2.751 (3)	154.4 (4)
	1.867 (-)	2.7491 (7)	149.9 (-)
	1.847 (-)	2.7491 (7)	154.0 (-)
N4—H14···O*w*^{vii}	1.895 (5)	2.887 (2)	166.8 (4)
	1.867 (-)	2.8780 (7)	165.9 (-)
	1.883 (-)	2.8790 (6)	166.7 (-)
N3—H12···O6^{vi}	1.991 (5)	2.926 (2)	151.4 (3)
	1.982 (-)	2.9226 (6)	150.1 (-)
	1.982 (2)	2.9225 (6)	151.7 (-)
N2—H11···O6^{vi}	2.171 (6)	3.070 (3)	145.1 (4)
	2.183 (-)	3.0620 (5)	141.9 (-)
	2.172 (-)	3.0619 (5)	144.0 (-)
N3—H13···O1^{vi}	2.577 (6)	3.434 (3)	142.0 (4)
	2.506 (-)	3.4174 (7)	146.8 (-)
	2.556 (-)	3.4167 (7)	141.9 (-)

Symmetry codes: (i) x, y, z; (ii) $-x, \frac{1}{2}+y, -z$; (iii) $1-x, \frac{1}{2}+y, -z$; (iv) $2-x, \frac{1}{2}+y, 1-z$; (v) $1+x, y, z$; (vi) $x, 1+y, z$; (vii) $1-x, y-\frac{1}{2}, 1-z$.

$-16(2) \times 10^{-8}$, leading to a mosaic spread of 41 (1), 46 (1) and 11.2 (1) s for g_{11}, g_{22} and g_{33}, respectively. The higher extinction value was $y = 0.318$ for the (003) reflection (F_o = 8.01 and F_c = 6.99 after correction). The rigid-bond test (Hirshfeld, 1976) was satisfactory, the maximum discrepancy being $\Delta = 0.0025$ Å^2 for the N4—C6 bond and average $<\Delta> = 0.0011$ Å^2 for non-H atoms. Bond distances and angles, as well as the most relevant intermolecular interactions, are given in the comparative Tables 3 and 4, respectively.

Table 5. *Fractional coordinates ($\times 10^5$) and anisotropic thermal parameters ($\times 10^5$ Å^2) for non-H atoms from the X–(X + N) model; fractional coordinates ($\times 10^4$) and anisotropic thermal parameters ($\times 10^3$ Å^2 for H atoms from the neutron refinement into the X-ray unit cell*

The form of the temperature factor is

$$T = \exp\left(-2\pi^2 \sum_i \sum_j h_i h_j a^{*i} a^{*j} U^{ij}\right).$$

	x	y	z	U_{11}	U_{22}	U_{33}	U_{12}	U_{13}	U_{23}
P	17786 (1)	−75000	−1107 (1)	780 (3)	584 (3)	1202 (3)	−56 (2)	38 (2)	20 (3)
O1	853 (6)	−84209 (6)	1752 (5)	1156 (11)	1300 (12)	2260 (15)	−359 (10)	637 (11)	−157 (11)
O2	35329 (6)	−84978 (6)	1194 (5)	945 (9)	975 (10)	1614 (12)	164 (8)	−29 (9)	−6 (9)
O3	13315 (7)	−69586 (7)	−15418 (5)	1565 (12)	1409 (12)	1305 (12)	−458 (10)	−370 (10)	263 (10)
O4	20953 (7)	−58196 (6)	6592 (5)	1662 (13)	867 (10)	1824 (14)	70 (10)	−239 (11)	−392 (10)
O5	92775 (5)	−83471 (5)	36144 (3)	1713 (11)	1199 (11)	2050 (12)	−145 (10)	−778 (11)	228 (10)
O6	68797 (4)	−94676 (4)	23725 (3)	1216 (9)	827 (9)	1609 (11)	−131 (8)	−84 (9)	−36 (8)
Ow	84440 (6)	−8289 (6)	52299 (5)	1216 (13)	1344 (14)	2108 (18)	204 (12)	5 (13)	15 (14)
N1	68588 (5)	−68226 (5)	7540 (3)	1099 (11)	941 (10)	1083 (11)	−29 (9)	162 (9)	−26 (9)
N2	49755 (5)	−22289 (5)	37153 (4)	940 (11)	994 (11)	1459 (13)	−5 (9)	118 (10)	11 (10)
N3	30748 (7)	−6269 (5)	22997 (4)	1519 (13)	1623 (13)	2019 (14)	60 (11)	139 (11)	788 (12)
N4	18782 (5)	−29491 (5)	31825 (3)	1120 (11)	1718 (12)	1825 (13)	−334 (10)	−296 (10)	598 (11)
C1	79568 (4)	−82612 (4)	27523 (3)	1004 (10)	794 (10)	1276 (11)	15 (8)	−57 (9)	−34 (9)
C2	75441 (5)	−65494 (4)	21055 (3)	925 (11)	776 (10)	1187 (12)	−16 (8)	92 (9)	−34 (9)
C3	61140 (5)	−55419 (5)	27092 (4)	1042 (11)	1066 (12)	1198 (12)	135 (10)	38 (10)	−138 (10)
C4	69048 (5)	−47933 (5)	39748 (3)	1001 (11)	1207 (12)	1098 (12)	165 (10)	50 (9)	−40 (10)
C5	55155 (5)	−36764 (5)	45212 (3)	1073 (11)	1299 (12)	1050 (12)	115 (10)	156 (9)	−20 (10)
C6	33123 (5)	−19594 (4)	30715 (3)	1065 (11)	1070 (11)	1141 (10)	−7 (9)	101 (9)	100 (10)
H1	8868 (5)	−5841 (6)	2154 (4)	20 (1)	19 (2)	34 (2)	−5 (1)	6 (1)	−3 (2)
H2	7897 (5)	−7437 (6)	353 (3)	26 (2)	23 (2)	26 (2)	5 (1)	11 (1)	−5 (1)
H3	6626 (5)	−5647 (5)	328 (3)	31 (2)	15 (1)	22 (2)	1 (2)	2 (1)	1 (1)
H4	5650 (5)	−7551 (6)	630 (3)	24 (2)	21 (2)	24 (2)	−8 (1)	1 (1)	−1 (1)
H5	4920 (5)	−6359 (6)	2812 (4)	22 (2)	32 (2)	37 (2)	−9 (2)	8 (2)	−8 (2)
H6	5648 (6)	−4510 (6)	2075 (4)	39 (2)	19 (2)	26 (2)	12 (2)	4 (2)	2 (1)
H7	7361 (6)	−5805 (6)	4658 (4)	37 (2)	25 (2)	26 (2)	10 (2)	1 (2)	5 (2)
H8	8146 (5)	−4029 (6)	3879 (4)	25 (2)	25 (2)	36 (2)	−7 (2)	11 (2)	−3 (2)
H9	4308 (5)	−4408 (6)	4665 (4)	23 (2)	26 (2)	33 (2)	−2 (1)	7 (1)	6 (2)
H10	6141 (6)	−3197 (6)	5461 (3)	41 (2)	35 (2)	13 (1)	3 (2)	−3 (1)	−10 (2)
H11	5994 (5)	−1371 (6)	3613 (4)	22 (2)	21 (2)	44 (2)	−6 (1)	1 (2)	6 (2)
H12	4188 (6)	87 (6)	2153 (4)	30 (2)	24 (2)	39 (2)	−6 (2)	6 (2)	10 (2)
H13	1794 (6)	−307 (6)	1895 (5)	28 (2)	34 (2)	55 (3)	9 (2)	−3 (2)	19 (2)
H14	1967 (6)	−3998 (6)	3728 (4)	30 (2)	19 (2)	39 (2)	−5 (2)	−2 (2)	9 (2)
H15	670 (5)	−2691 (6)	2618 (4)	20 (2)	34 (2)	44 (2)	−7 (2)	−12 (2)	11 (2)
H16	9053 (6)	−171 (6)	4652 (4)	28 (2)	28 (2)	34 (2)	0 (2)	5 (2)	4 (2)
H17	9347 (5)	−1664 (6)	5635 (4)	28 (2)	19 (2)	40 (2)	7 (2)	−1 (2)	2 (2)
H18	2121 (5)	−6043 (5)	−1847 (4)	29 (2)	21 (2)	26 (2)	−5 (1)	1 (2)	3 (1)
H19	1161 (5)	−4917 (5)	407 (4)	30 (2)	13 (2)	38 (2)	6 (1)	7 (2)	−1 (2)

5. X–X and X–(X + N) least-squares refinements

As pointed out above, both refinements were performed against the anomalous dispersion-corrected 2/*m* symmetry-averaged data set. Chemically equivalent O and N atoms were constrained to have the same multipole parameters (O1 = O2, O3 = O4, O5 = O6 and N3 = N4). Symmetries 2 for P, *m* for O5, O6, N3 and N4, and *mm* for C1 and C6 were also imposed. Electron-density parameters of the H atoms were not chemically constrained. Local axes, radial function parameters and multipolar orders of pseudo-atoms were defined as previously (Fig. 1); in the X–(X+N) model the three dipole parameters of each H atom were refined. The Becker–Coppens extinction model (Becker & Coppens, 1974; isotropic Lorentz type I) was applied in both cases. The extinction was found to be insignificant.

5.1. X—X refinement

Starting parameters for non-H atoms were taken from HO refinement. The multipolar refinement strategy ($0 < \sin\theta/\lambda < 1.2$ Å^{-1}) was the following: (*a*) scale factor, (*b*) P_v then κ (until convergence), (*c*) P_v and P_{lm}, (*d*) κ, G (extinction parameter) and P_{lm}, (*e*) positional and U_{ij} parameters for non-H atoms and P_{lm} and (*f*) κ', and this process was cycled until total convergence. After each heavy atom *xyz* refinement, the H-atom coordinates were shifted according to neutron values and hydrogen isotropic thermal motion was adjusted ($\sin\theta/\lambda < 0.5$ Å^{-1}). An anharmonicity model was tested, with fourth-order Gramm–Charlier cumulants for the P atom and third-order cumulants for O1, O2, O3, O4, O5, O6 and C1 atoms. This latter refinement did not lead to better statistical indices or more meaningful density

maps, therefore, it was rejected. The rigid-bond test was applied for non-H atoms at the end of the refinement: the maximum discrepancy is $\Delta = 6 \times 10^{-4}$ Å^2 for the N2—C5 bond and an average $<\Delta> = 2.1 \times 10^{-4}$ Å^2. We therefore conclude that deconvolution between thermal and electron density parameters is excellent. Furthermore, this test is much better than that calculated from the neutron model, in spite of the highest number of refined parameters. Thus, the greatest accuracy of non-H thermal parameters is reached with X-ray data through a multipolar refinement. Table 2 gives the statistical indices at the convergence. As expected from rigid-bond test results, S was much better in X–X than in the neutron model. Bond distances and angles as well as most relevant intermolecular interactions are given in Tables 3 and 4, respectively.

5.2. *X*–(*X* + *N*) *refinement*

The disagreement between the two diffraction experiments concerning the rigid-bond test results did not allow any transferability of non-H parameters from a neutron model to an X-ray model. Thus, as in most studies only positional and anisotropic thermal parameters of H atoms from the neutron experiment were included in the X–($X+N$) refinement. As Craven and collaborators usually do (Epstein, Ruble & Craven, 1982), quadrupolar harmonic functions for H atoms were tested in this refinement but without significant improvement; therefore, only dipolar functions were used. Statistical factors of HO X–($X + N$) refinement were $R = 0.030$, $R_w = 0.029$ and $S = 1.23$ for 2973 observed reflections [$I > 3\sigma(I)$]. The same X–X refinement strategy except for H atoms (xyz and U_{ij} parameters fixed at neutron values in the X-ray unit cell) was applied to the same X-ray data set. The rigid-bond test was applied for non-H atoms at the end of the refinement with a maximum discrepancy of $\Delta = 6 \times 10^{-4}$ Å^2 for the N2—C5 bond and an average $<\Delta> = 2.3 \times 10^{-4}$ Å^2. The deconvolution was as effective as for the X–X refinement. As shown in Table 2 (which compared both X-ray models) the statistical indices in X–($X + N$) become systematically smaller when neutron parameters of H atoms are introduced. Bond distances and angles as well as most relevant intermolecular interactions are given in the comparative Tables 3 and 4, respectively. Table 5 shows all positional and thermal parameters from X–($X + N$) refinement. Fig. 2 gives the observed electron density deformation in the O1—P—O3 and N3—C6—N4 sections [X–($X+N$) model]; the corresponding maps for the X–X model are given in the supplementary material.*

These experimental dynamic deformation maps were calculated as defined previously (Coppens, 1982). The Fourier summation included 3832 F_o's with $\sin\theta/\lambda < 0.9$ Å^{-1} and $I > 3\sigma(I)$. These maps give an estimation of the quality of measurements and include the effects of both finite experimental resolution and convolution with the atomic thermal parameters. Internal and external estimates of the average error in the experimental deformation maps (Cruickshank, 1949) are 0.02 and 0.08 e Å^{-3}, respectively.*

* See deposition footnote.

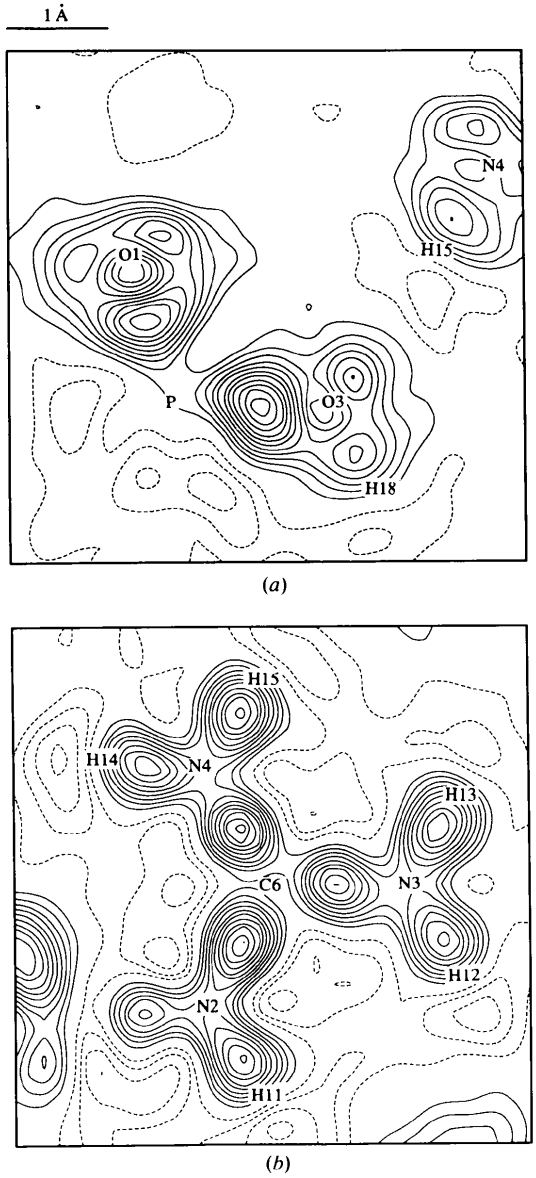

Fig. 2. Observed deformation electron density in the sections (*a*) O1—P—O3 and (*b*) N3—C6—N4 [X–($X + N$) model, 3832 reflections, $\sin\theta/\lambda < 0.9$ Å^{-1}, $I > 3\sigma(I)$]. Contour intervals are at 0.05 e Å^{-3}; solid lines positive, dotted lines negative and zero contour omitted.

* Lists of structure factors, anisotropic displacement parameters, neutron fractional coordinates, X–X fractional coordinates, X–X and X–($X + N$) electron density parameters, and rigid-bond test results for neutron, X–X and X–($X + N$) displacement paramters have been deposited with the IUCr (Reference: PA0310). Copies may be obtained through The Managing Editor, International Union of Crystallography, 5 Abbey Square, Chester CH1 2HU, England.

6. Structural results

6.1. *Crystal packing*

Bond distances and angles for neutron, *X–X* and *X–(X + N)* models are given in Table 3. Intermolecular interactions for the three models are listed in Table 4. Fig. 3 gives the *ORTEP*II view (Johnson, 1976) of the formula unit and Fig. 4 is a slice of the structure at both sides of the (001) section [*X–(X + N)* coordinates]. According to Aoki, Nagano & Iitaka (1971), the crystal structure of LAP may be described as layers of phosphate ions, arginine ions and water molecules held together by hydrogen bonds and stacked along the *c* axis [*c* = 10.779 (3) Å]. We can also describe LAP by almost coplanar $H_2PO_4^-$ and NH_3^+ groups linked together by hydrogen bonds and coulombic interactions, as shown in Fig. 4 and Table 4. This arrangement is similar to that observed in the ammonium dihydrogen phosphate [ADP (Tenzer, Frazer & Pepinsky, 1958)]. In LAP

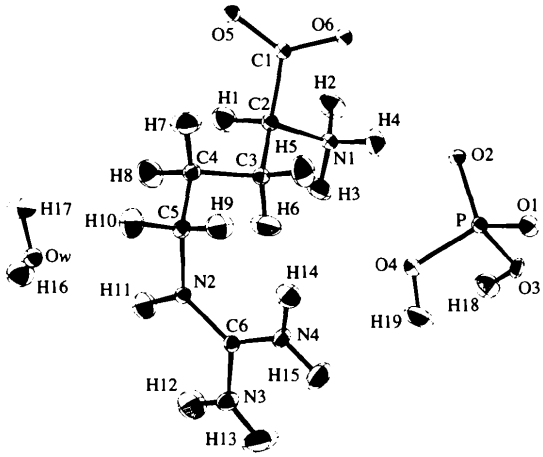

Fig. 3. *ORTEP* (Johnson, 1976) view of the asymmetric unit in LAP [*X–(X + N)* model]. Thermal ellipsoids are at the 50% probability level.

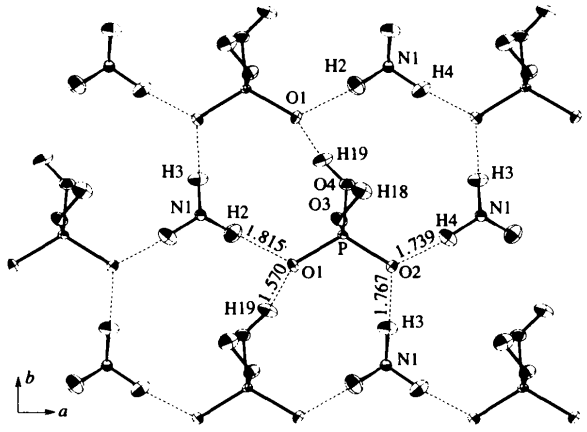

Fig. 4. *ORTEP* (Johnson, 1976) view of a thin layer of phosphates and amino groups at both sides of the (001) plane [*X–(X + N)* model].

Table 6. *Maximum and minimum phosphate group bond distances (Å) and angles (°) in* LAP_{RT}, LHP_{H_2O}, $LHP_{H_3PO_4}$, *ImP and ADP (respectively, L-arginine phosphate monohydrate at room temperature, L-histidine phosphate monohydrate, L-histidine phosphate crystallized with a phosphoric acid molecule, imidazole phosphate and ammonium dihydrogen phosphate);* $O\cdots O^{intra}$ *and* $O\cdots O^{inter}$ *are intra- and intermolecular distances, respectively*

	LAP 130 K	LAP_{RT}	LHP_{H_2O}	$LHP_{H_3PO_4}$	ImP	ADP 138 K
P—O	1.4981	1.495	1.509	1.510	1.495	1.5160
	1.5062	1.500	1.514	1.518	1.503	1.5208
P—O(H)	1.5673	1.564	1.561	1.547	1.544	1.5627
	1.5901	1.585	1.579	1.551	1.555	1.5690
$O\cdots O^{intra}$	2.4635	2.450	2.470	–	–	2.479
	2.5450	2.539	2.535	–	–	2.543
$O\cdots I^{inter}$	2.5604	2.568	2.555	2.460	2.557	2.495
				2.583	2.591	
O—P—O	114.95	115.23	113.9	113.4	114.3	112.34
					115.7	
HO—P—OH	106.27	106.34	104.56	107.7	105.0	104.64
					107.6	
O—P—OH	105.39	105.09	106.9	106.6	106.3	107.17
	111.53	111.72	111.0	112.5	111.4	109.84

these compact planes are linked together by the carboxyl group *via* the water molecule. Phosphate groups are linked together by means of the strongest interaction O4—H19···O1 [H19···O1 = 1.570, O4···O1 = 2.5604 (7) Å], whereas hydrogen bonds between amino and phosphate groups (N1—H4···O2, N1—H3···O2′ and N1—H2···O1) range from 1.739 to 1.815 Å. $H_2PO_4^-$ and NH_3^+ ions lie at both sides of the (001) plane. The H18 atom links the phosphate anion to the carboxyl group by means of a very strong hydrogen bond [H18···O6 = 1.589, O3···O6 = 2.5939 (6) Å]. Inside the unit cell water molecules are arranged along the 2_1 axis, linking arginine molecules through their carboxyl groups [O5···H16—O*w*—H17···O5′]. Surrounding the roughly planar guanidinium group lie several O atoms, making other hydrogen bonds (see Table 4). Therefore, this strong hydrogen-bond network and numerous short contacts lead to a rigid structure, with two sections of high electron density and strong coulombic interactions [(001) plane and guanidinium mean plane].

6.2. *The phosphate group*

As discussed by Blessing (1986), conformational geometry and O···O intramolecular and intermolecular distances keep many similarities in phosphate salts. Table 6 shows structural results from several phosphate salts that have been solved (LAP_{RT}: Espinosa, 1994; LHP_{H_2O}: Espinosa, Molins, Veintemillas & Miravitlles, 1995; $LHP_{H_3PO_4}$ and ImP: Blessing, 1986; ADP: Boukhris, Souhassou, Lecomte & Kempf, 1994). In all cases the distortion of the PO_4 tetrahedron is very

small, the O···O distances being equal within 0.1 Å in spite of the existence of different P—O bonds [P—O and P—O(H)].

7. Comparative discussion between *X–X* and *X–(X + N)* models

The first *X–N* study was made by Coppens (1967); then several comparative *X–X* and *X–N* studies were performed; the most relevant ones were performed on oxalic acid under a Sagamore Commission Project (Coppens *et al.*, 1984). However, to our knowledge, the resulting electrostatic properties, which are one of the aims of this paper, were never compared.

7.1. *Structural parameters*

Comparative tables for fractional coordinates, thermal parameters, bond distances, angles and intermolecular interactions [*X–X* and *X–(X+N)* models] show, for non-H atoms, no significant differences within their e.s.d.'s. A detailed comparison between *X–X*$_{HO}$ and neutron parameters has been published a long time ago (Hanson, Sieker & Jensen, 1973) and our results confirm this study.

7.2. *Electron density parameters*

The electron density parameters of the non-H atoms are statistically equal for both refinements [the highest discrepancy being $\Delta = 7\sigma$ for the valence population of the O5 (=O6) atom] and the resulting static densities and bond peak heights are equal within 0.05 e Å^{-3}. As expected, significant differences are found on the hydrogen population multipolar parameters. These differences are not clearly related to shifts in hydrogen coordinates: for example, whereas the change in the H6 dipole parameter is statistically significant along the bond direction ($\Delta = -0.09$ e), its bond distance only changes by 0.004 Å; on the other hand, the H10 dipolar parameter does not vary ($\Delta = 0.00$ e) for a 0.032 Å coordinate shift. Furthermore, due to the different thermal vibration models [isotropic for *X–X* and anisotropic for *X–(X+N)*] we cannot directly compare the atomic electron density parameters. Some significant changes appearing in the κ and κ' values are not in clear relation with other parameters.

7.3. *Electron density maps*

Fig. 5 shows *X–(X+N)* residual maps ($0 < \sin\theta/\lambda < 1.2$ Å^{-1}) in the O1—P—O3 and N3—C6—N4 planes; the corresponding *X–X* residual sections are given as supplementary material.* A residual density equal or less than 0.05 e Å^{-3} is found everywhere except around the P atom (maximum residual 0.15 e Å^{-3} for both models). Both refinements then succeed to fit the same observed electron density; Fig. 6 shows the *X–(X + N)* static electron-density deformation model in the O5—C1—O6, O1—P—O3 and N3—C6—N4 sections (see supplementary material for the *X–X* sections) as defined in (2) as

$$\Delta\rho_{\text{stat}}(\mathbf{r}) = \sum_{i=1}^{N_{at}} \Delta\rho_i(r) \qquad (2)$$

where

$$\Delta\rho_i(\mathbf{r}) = P_v\kappa^3\rho(\kappa r) - N_v\rho_v(r) + \sum_{l=0}^{l_{max}} \sum_{m=0}^{l} \kappa'^3 R_{nl}(\kappa' r) P_{lm\pm} y_{lm\pm}(\theta, \varphi)$$

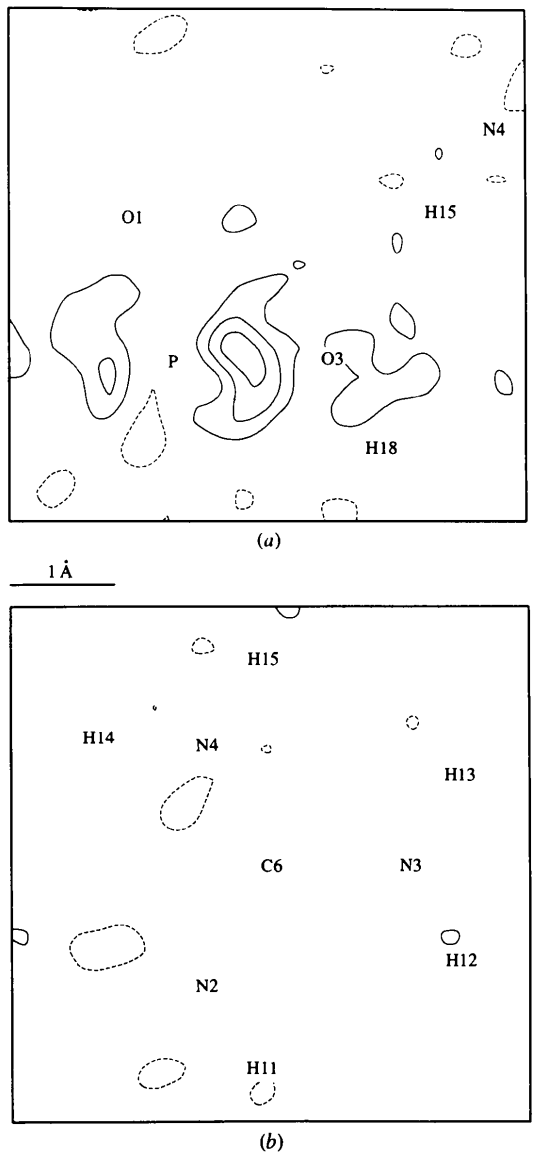

Fig. 5. Residual maps in (*a*) O1—P—O3 and (*b*) N3—C6—N4 planes [*X–(X + N)* refinement, 6805 reflections, $\sin\theta/\lambda < 1.2$ Å^{-1}, $I > 3\sigma(I)$]. Contours as in Fig. 2.

* See deposition footnote on p. 525.

and N_v is the free-atom valence electrons [for clarity the i index is omitted on the right side of (2)]. In both X–$(X+N)$ and X–X maps, oxygen lone pairs are contracted and slightly asymmetric (differences reach ~ 0.10 e Å^{-3} in both phosphate and carboxyl groups). This asymmetry remains in the perpendicular planes to the C—O and P—O directions at 0.3 Å out of the bond, where the most populated lone pair is also more extended, possibly resulting from a polarization due to the intermolecular interactions. Electron density peak heights for bonds and oxygen lone pairs in X–$(X+N)$ and X–X models are given in Table 7. For any bond which does not involve an H atom, electron density differences are less than or equal to 0.05 e Å^{-3}. O lone-pair density differences may reach 0.10 e Å^{-3} in some sections. It therefore seems that a better description of H atoms influences only slightly the lone-pair lobes, as can also be seen in each O···H—X map (X = O, N). A systematic increase of the bonding electron density involving H atoms is found in the X–$(X+N)$ model. The electron density bond values found in the X–$(X+N)$ model are in excellent agreement with those found in theoretical calculations of enkephaline (Wiest, Pichon-Pesme, Bénard & Lecomte, 1994) and phosphoric acid (Moss, Souhassou, Espinosa, Lecomte & Blessing, 1995), even if the chemical environment is not the same.

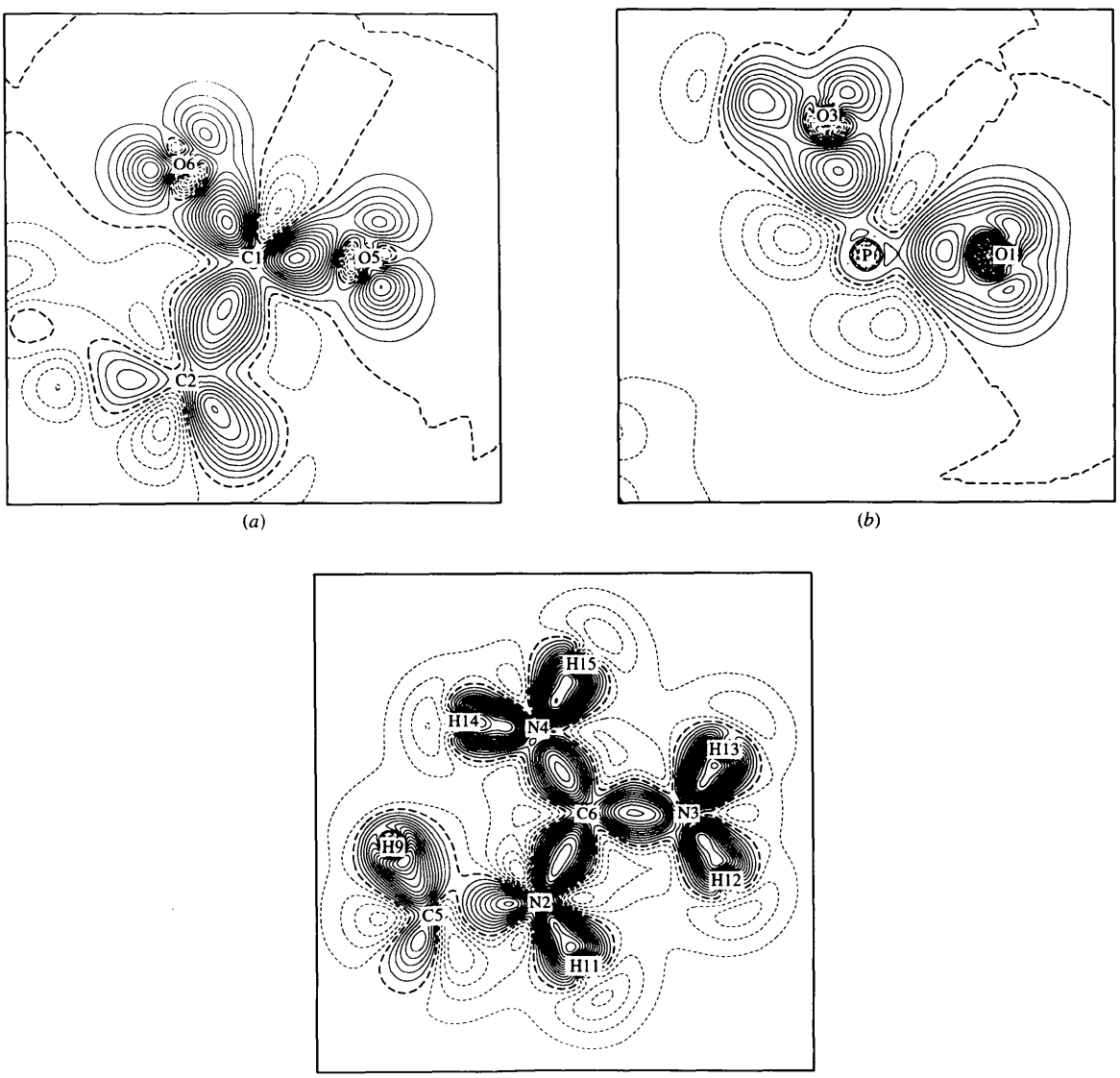

Fig. 6. Static electron density deformation in (*a*) O5—C1—C6, (*b*) O1—P—O3 and (*c*) N3—C6—N4 planes [X–$(X+N)$ model]. Contours as in Fig. 2; zero contour as broken lines.

Table 7. *Electron density bond peaks and lone-pair values (e Å^{-3}) from X–(X+N) and X–X models*

	X–(X+N)	X–X
P—O1(=O2)	0.50	0.45
P—O3(=O4)	0.50	0.50
C1—O5(=O6)	0.60	0.60
C1—C2	0.50	0.45
C2—N1	0.50	0.45
C2—C3	0.50	0.50
C3—C4	0.50	0.50
C4—C5	0.40	0.35
C5—N2	0.45	0.50
N2—C6	0.60	0.60
C6—N3(=N4)	0.55	0.55
H1—C2	0.80	0.65
H2—N1	0.80	0.80
H3—N1	0.75	0.65
H4—N1	0.80	0.75
H5—C3	0.65	0.50
H6—C3	0.80	0.50
H7—C4	0.75	0.50
H8—C4	0.75	0.45
H9—C5	0.70	0.50
H10—C5	0.85	0.60
H11—N2	0.70	0.50
H12—N3	0.70	0.65
H13—N3	0.85	0.60
H14—N4	0.75	0.65
H15—N4	0.80	0.60
H16—O*w*	0.65	0.40
H17—O*w*	0.50	0.35
H18—O3	0.45	0.25
H19—O4	0.50	0.30
Lone pairs	X–(X+N)	X–X
O1 (O1···H19—O4)	0.45	0.45
O1 (O1···H2—N1)	0.50–0.40	0.40–0.45
O2 (O2···H4—N1)	0.45	0.45
O2 (O2···H3—N1)	0.45	0.45
O3 (O3···H15—N4)	0.40	0.45
O5 (O5···H17—O*w*)	0.40	0.35
O5 (O5···H16—O*w*)	0.25	0.25
O6 (O6···H18—O3)	0.15	0.15
O6 (O6···H12—N3)	0.40	0.35
O6 (O6···H11—N2)	0.25	0.20
O*w* (O*w*···H14—N4)	0.25	0.20

Table 8. *Atomic net charges (in e), κ's and charges of molecular groups from κ refinements; Δ is the difference between the two refinements*

	X–(X+N)		X–X	
	κ	q	κ	q
P	1.015	+0.44 (5)	1.022	+0.43 (5)
O1	0.965	−0.60 (2)	0.968	−0.54 (1)
O2	0.971	−0.58 (2)	0.976	−0.48 (1)
O3	0.974	−0.50 (1)	0.972	−0.49 (1)
O4	0.974	−0.49 (1)	0.975	−0.44 (1)
O5	0.984	−0.41 (1)	0.986	−0.36 (1)
O6	0.981	−0.44 (1)	0.986	−0.34 (1)
O*w*	0.969	−0.69 (2)	0.979	−0.54 (2)
N1	0.985	−0.66 (2)	0.979	−0.77 (3)
N2	1.011	−0.30 (3)	1.009	−0.30 (3)
N3	0.984	−0.67 (1)	0.976	−0.66 (2)
N4	0.982	−0.80 (1)	0.974	−0.83 (2)
C1	1.050	+0.15 (3)	1.059	+0.35 (2)
C2	1.016	−0.25 (4)	1.020	−0.13 (4)
C3	1.013	−0.34 (4)	1.024	−0.29 (4)
C4	1.017	−0.11 (4)	1.006	−0.04 (5)
C5	1.000	−0.39 (4)	1.001	−0.31 (4)
C6	1.071	+0.48 (3)	1.087	+0.62 (3)
H1	1.405	+0.22 (2)	1.183	+0.11 (2)
H2	1.287	+0.30 (2)	1.138	+0.30 (3)
H3	1.604	+0.48 (2)	1.316	+0.44 (2)
H4	1.489	+0.45 (2)	1.343	+0.49 (2)
H5	1.214	+0.12 (3)	1.053	+0.12 (3)
H6	1.380	+0.32 (2)	1.148	+0.25 (3)
H7	1.300	+0.11 (2)	1.119	+0.10 (3)
H8	1.330	+0.10 (2)	1.101	+0.03 (2)
H9	1.331	+0.24 (2)	1.121	+0.18 (3)
H10	1.303	+0.21 (2)	1.105	+0.18 (3)
H11	1.274	+0.27 (3)	1.101	+0.22 (3)
H12	1.526	+0.40 (2)	1.154	+0.30 (2)
H13	1.606	+0.40 (2)	1.203	+0.31 (2)
H14	1.474	+0.42 (2)	1.217	+0.42 (3)
H15	1.479	+0.40 (2)	1.197	+0.32 (2)
H16	1.368	+0.39 (2)	1.055	+0.24 (2)
H17	1.231	+0.30 (2)	1.118	+0.31 (2)
H18	1.305	+0.42 (2)	1.109	+0.32 (3)
H19	1.547	+0.54 (2)	1.245	+0.50 (2)

Group	Σq(X–(X+N))	Σq(X–X)	Δ
H_2PO_4	−0.77	−0.70	−0.07
COO	−0.70	−0.45	−0.25
NH_3	+0.57	+0.46	+0.11
H_2O	+0.00	−0.01	+0.01
$NH—C—(NH_2)_2$	+0.60	+0.40	+0.20
$CH—(CH_2)_3$	+0.23	+0.20	+0.03

7.4. *Net charges and dipole moment*

In order to compare associated atomic net charges, a κ refinement (Coppens *et al.*, 1979) was performed for both models (see Table 2 for agreement factors). No constraints on any atom were imposed. Table 8 gives the net charges of atoms and molecular groups obtained from the two models.

The κ values of non-H atoms are in close agreement for both refinements. Oppositely, those of H atoms increase systematically by 20–30% from *X–X* to *X–(X + N)* refinement, showing a more contracted electron density. This result is in relation to the thermal motion model of H atoms: in the *X–X* refinement H-atom isotropic *U*s are systematically smaller than those of *X–(X + N)*. We did not find any systematic trend when charges are compared: H atom charges agree generally within 0.1 e, the largest discrepancy is 0.11 e for H1. Larger discrepancies between non-H atoms appear: for example, the charge of C1 is 0.15 e in *X–(X + N)* refinement compared with 0.35 e in *(X–X)*; C6 varies from 0.48 to 0.62 e. This results in some differences between group net charges reaching 0.25 e for the COO^- group. It is therefore difficult to derive definitive conclusions. Moreover, it is surprising to see that the major discrepancies occur on non-H atoms and precisely on C1 and C6, which are not linked to H atoms. Both *X–X* and *X–(X+N)* refinements converged very well, but both had some weakness: in the *X–X* model the isotropic

thermal motion of H atoms (which is correlated to κ's) leads to uncertainties; in the X–(X+N) model the neutron refinement is not entirely satisfactory (because the rigid bond test led to a worse agreement than that made from X–X thermal parameters). On the other hand, as shown later, the electrostatic potential calculated from both refinements agrees very well with the van der Waals surface of the molecule.

The dipole moments (μ's) shown in Table 9 were calculated from both κ and multipolar refinements with X–X and X–(X + N) data according to the expressions

$$\boldsymbol{\mu}_\kappa = \sum_{i=1}^{N_{at}} (Z_i - P_{vi})\mathbf{r}_i$$

$$\boldsymbol{\mu}_{\text{multipolar}} = \sum_{i=1}^{N_{at}} \left\{ (Z_i - P_{vi})\mathbf{r}_i - [4(n_{li}+3)/3\kappa_i'\zeta_i] \times (\mathbf{abc})\mathbf{RT}_i \begin{pmatrix} P_{11} \\ P_{1\bar{1}} \\ P_{10} \end{pmatrix}_i \right\},$$

where the sums are over all atoms in the neutral asymmetric unit, Z_i is the positive atomic charge, r_i is

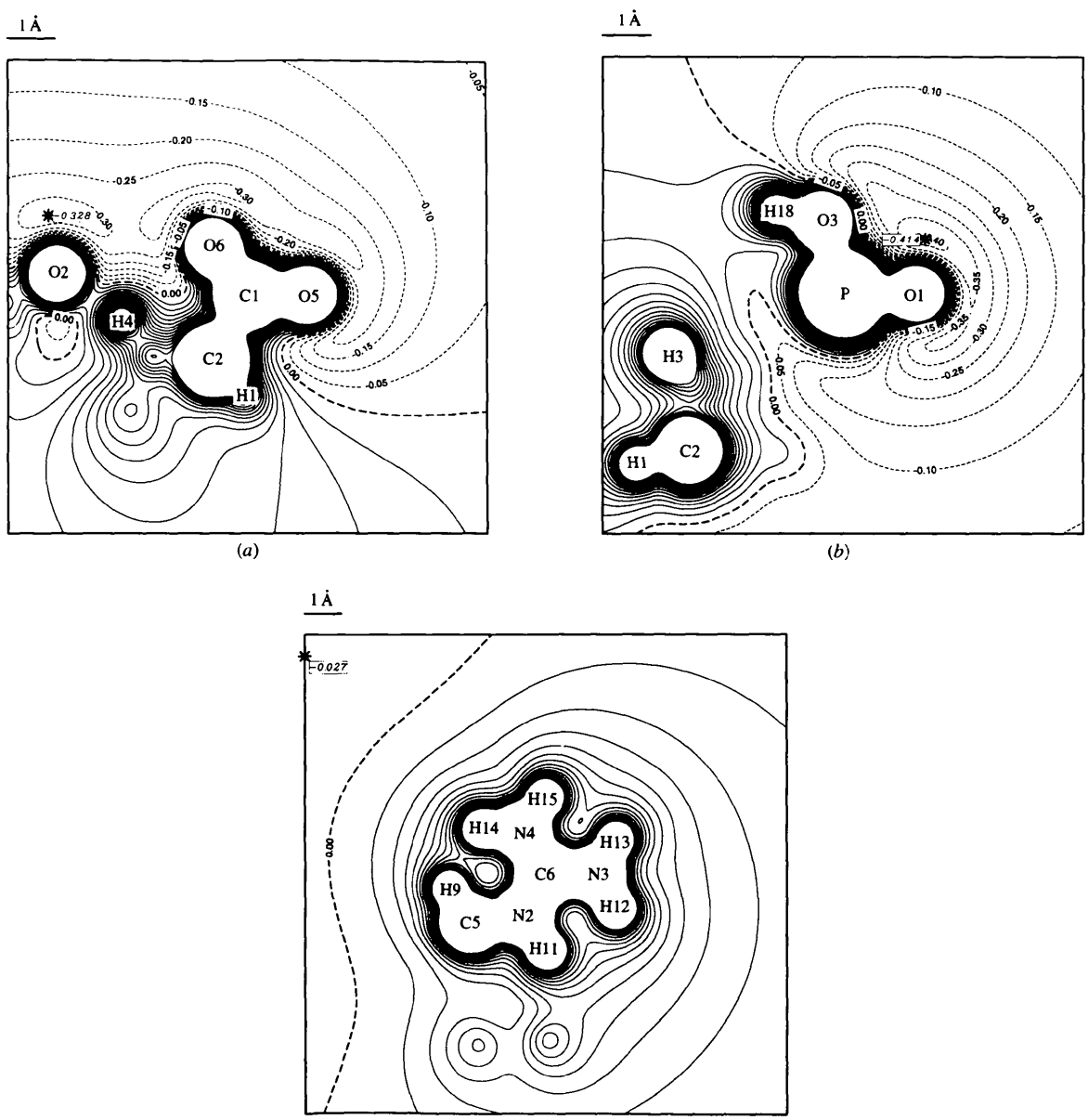

Fig. 7. Electrostatic potential around a pseudo-isolated molecule from the X–(X + N) model in (*a*) O5—C1—O5, (*b*) O1—P—O3 and (*c*) N3—C6—N4 planes. Contour intervals are at 0.05 e Å^{-1}; solid lines positive, dotted lines negative and zero contour as broken lines. The minimum value on each plot is marked by '*'.

Table 9. *Dipole moment components (in crystal axis system), dipole moment modulus and angle formed between the dipole moment vector and the* **b** *polar axis from multipolar and κ refinements in X–(X + N) and X–X models*

Group	Refinement	Model	μ_a (D)	μ_b (D)	μ_c (D)	μ_d (D)	α (°)
	Multipolar	*X*–(*X* + *N*)	4.8	29.0	5.2	30 (2)	15.1
$H_2PO_4^-.Arg^+.H_2O$		*X*–*X*	2.6	23.4	4.7	24 (2)	15.6
(Asymmetric unit)	κ	*X*–(*X* + *N*)	1.4	31.9	0.9	32 (2)	3.0
		X–*X*	3.3	21.5	2.7	22 (2)	11.7

Table 10. *Topological characterization of the electron density for selected critical points in LAP: bond distances (d_1, d_2 Å) to each atom, fractional coordinates (xyz), curvatures (λ_1, λ_2, λ_3), Laplacian ($\nabla^2\rho$ e Å^{-5}), electron density (ρ e Å^{-3}) and ellipticity (ε) values at each CP from X–(X + N) (top) and X–X models*

CP	(1)	(2)	d_1	d_2	*xyz*	$\lambda_1, \lambda_2, \lambda_3$	$\nabla^2\rho$	ρ	ε
1	C2	C1	0.752	0.782	0.773,−0.739,0.243	10.69,−10.22,−11.61	−11.15	1.63	0.14
(3,−1)			0.748	0.787	0.772,−0.739,0.242	10.04,−9.84,−11.77	−11.57	1.60	0.20
2	C1	O5	0.497	0.748	0.849,−0.829,0.309	24.69,−21.99,−25.76	−23.06	2.70	0.17
(3,−1)			0.494	0.751	0.848,−0.830,0.309	23.89,−21.66,−25.91	−23.69	2.68	0.20
3	C1	O6	0.517	0.752	0.752,−0.875,0.260	23.02,−20.70,−24.25	−21.93	2.61	0.17
(3,−1)			0.514	0.755	0.753,−0.876,0.260	21.92,−20.36,−24.36	−23.69	2.59	0.20
4	P	O1	0.617	0.890	0.107,−0.786,0.000	38.83,−10.94,−11.64	16.25	1.68	0.06
(3,−1)			0.621	0.887	0.107,−0.787,0.000	37.82,−10.38,−11.40	16.04	1.62	0.10
5	P	O3	0.643	0.948	0.161,−0.728,−0.069	26.35,−8.82,−10.61	6.93	1.46	0.20
(3,−1)			0.642	0.949	0.162,−0.729,−0.069	26.47,−8.74,−10.30	7.44	1.46	0.18
6	C6	N3	0.586	0.753	0.320,−0.138,0.273	17.31,−16.16,−20.21	−19.06	2.30	0.25
(3,−1)			0.586	0.752	0.321,−0.138,0.273	16.35,−16.12,−19.83	−19.59	2.30	0.23
7	C6	N4	0.577	0.751	0.270,−0.240,0.313	17.23,−16.63,−20.71	−20.12	2.34	0.25
(3,−1)			0.578	0.751	0.270,−0.240,0.313	16.20,−16.60,−20.29	−20.70	2.34	0.22
8	C6	N2	0.576	0.755	0.403,−0.208,0.335	18.25,−16.63,−22.05	−20.43	2.39	0.33
(3,−1)			0.576	0.755	0.403,−0.208,0.335	17.78,−16.39,−21.63	−20.24	2.37	0.32
9	C5	N2	0.611	0.847	0.528,−0.308,0.418	14.74,−10.75,−11.91	−7.92	1.63	0.11
(3,−1)			0.609	0.850	0.527,−0.309,0.417	15.35,−10.16,−11.75	−6.56	1.59	0.16
10	H9	C5	0.378	0.708	0.471,−0.413,0.461	18.45,−15.58,−16.49	−13.62	1.73	0.06
(3,−1)			0.319	0.766	0.464,−0.414,0.464	13.68,−15.29,−15.89	−17.50	1.66	0.04
11	H11	O6	0.869	1.388	0.597,−0.069,0.298	1.89,−0.22,−0.27	1.39	0.06	0.23
(3,−1)			0.864	1.366	0.610,−0.069,0.302	1.93,−0.28,−0.33	1.32	0.08	0.21
12	H12	O6	0.709	1.289	0.516,0.011,0.227	3.14,−0.42,−0.46	2.26	0.10	0.10
(3,−1)			0.723	1.284	0.517,0.012,0.231	2.90,−0.44,−0.48	1.98	0.11	0.10
13	H9	O*w*	0.915	1.411	0.319,−0.493,0.466	1.65,−0.23,−0.27	1.15	0.07	0.19
(3,−1)			0.936	1.393	0.318,−0.495,0.468	1.57,−0.25,−0.27	1.05	0.08	0.11
14	H14	O*w*	0.646	1.253	0.169,−0.456,0.410	3.87,−0.59,−0.72	2.57	0.14	0.23
(3,−1)			0.619	1.275	0.168,−0.459,0.403	3.58,−0.38,−0.50	2.70	0.11	0.30
15	H15	O3	0.616	1.222	0.004,−0.249,0.221	4.78,−0.58,−0.68	3.52	0.15	0.17
(3,−1)			0.612	1.226	0.007,−0.239,0.223	4.38,−0.49,−0.57	3.32	0.14	0.15
16	H11	H12	1.127	1.170	0.542,−0.057,0.279	0.73,0.34,−0.16	0.92	0.05	-
(3,+1)			1.174	1.169	0.540,−0.054,0.278	0.65,0.44,−0.18	0.91	0.06	-
17	H14	H9	0.971	1.066	0.286,−0.452,0.437	0.73,0.39,−0.20	0.93	0.06	-
(3,+1)			0.894	1.130	0.277,−0.454,0.432	0.77,0.42,−0.18	1.02	0.06	-
18	H14	H9							
(3,−1)			0.994	1.044	0.330,−0.372,0.405	1.98,−0.14,−0.41	1.42	0.12	1.97
19	H14	H9							-
(3,+1)			1.075	1.107	0.338,−0.357,0.400	1.83,0.16,−0.39	1.60	0.12	-

the atomic position and P_{vi}, n_{li}, κ_i' and ζ_i were defined previously; the column vector $(P_{11}P_{1\bar{1}}P_{10})_i$ is the dipole vector $\mathbf{d}_i$ of the i atom in the local atomic orthogonal system, $\mathbf{T}_i$ is its associated matrix to transform $\mathbf{d}_i$ into the (**ab*c****) orthogonal system where all atomic dipoles are added and **R** is the transformation matrix from the (**ab*c****) system to the (**abc**) crystallographic axis system. Because of the definition of multipolar population in the *MOLLY* program, the second term is negative. We note that the dipolar term of the electron density corrects a part of the effort made on the position of the H atoms for the *X*–*X* model.

We have observed a systematic increase in the modulus of $\boldsymbol{\mu}$ when *X*–(*X* + *N*) parameters are used. Multipolar refinement leads to better agreement than κ only refinement, for both the α angle between $\boldsymbol{\mu}$ and the 2_1 axis and for the moduli. In LAP the atomic net charges obtained in the κ refinement of the *X*–(*X* + *N*) model strengthen the polarity inside of the phosphate, water and arginine groups, increasing the dipolar moment in the asymmetric unit. In both multipolar *X*–*X* and *X*–(*X* + *N*) refinements the net charge contribution is much greater than the atomic dipoles contribution ($\sim$ 2 debeye). The large modulus

of the dipole moment in the asymmetric unit and its small angle with the crystal b axis is mainly due to the phosphate contribution: the direction of the $H_2PO_4^-$ dipole remains roughly along the b polar axis ($\alpha \simeq 10°$) and its modulus is preponderant due to its high polarity. Therefore, the structural arrangement of phosphate groups [lying at both sides of the (001) plane], their close and strong interactions, and their high contribution to the dipole moment in the asymmetric unit are totally coherent. The dipole moment of the neutral water molecule was found to be 1.92 (9) and 1.54 (5) debeye in the X–($X + N$) and X–X κ refinement models, respectively. These values are within the range of those found in the literature (Spackman, 1992); the first value is certainly better because of the neutron information.

7.5. *Electrostatic potential of a LAP entity removed from the crystal lattice*

Electrostatic potential calculations were performed using the *ELECTROS* program (Ghermani, Bouhmaida & Lecomte, 1992) around the pseudo-isolated molecule, *i.e.* all information on the molecular groups was obtained from the crystal but the electrostatic potential function was only calculated in the asymmetric unit. Fig. 7 gives the X–($X + N$) electrostatic potential calculations in the O5—C1—O6 (8*a*), O1—P—O3 (8*b*) and N3—C6—N4 (8*c*) sections. As expected, whereas a negative potential extends continuously from the carboxyl group to the $H_2PO_4^-$ anion, the guanidinium group develops a pocket of positive potential. The absolute minimum potential, close to H_2PO_4, is –0.42 e Å^{-1} corresponding to an energy of –583.5 kJ mol^{-1} for a positive unit point charge. A value of –0.33 e Å^{-1} corresponding to an energy of –458.4 kJ mol^{-1} for a positive unit point charge appears close to the carboxyl group. A similar calculation with the X–X parameters led essentially to the same values outside the molecular van der Waals surface ($\Delta V < 0.05$ e Å^{-1}). The related sections $\Delta V = V_{X-(X+N)} - V_{X-X}$ are deposited as supplementary material.*

7.6. *Topology of the electron density*

In order to carry out a topological analysis (Bader, 1990) of the experimental electron density from both X–($X + N$) and X–X models in several planes, we calculated the topology of $\rho(\mathbf{r})$ with the *PROP* program (Souhassou, 1992). The X–($X + N$) Laplacian maps in the O1—P—O3 and N3—C6—N4 sections are given in Fig. 8 and the topological analysis in the guanidinium group for both refinements appears in Table 10; the corresponding X–X maps are given in the supplementary material.* The locations and curvatures of the intramolecular critical points are in excellent agreement for both refinements. Destro, Bianchi, Gatti & Merati (1991) and Howard, Hursthouse, Lehmann & Poyner (1995) have recently discussed the topological features of L-alanine and one of its hydroxyphenyl derivatives (L-dopa) from X-ray data, using a modified version of the *VALRAY* set of programs (Stewart & Spackman, 1983) and *MOLLY* (Hansen & Coppens, 1978) models. Table 11 gives the comparison between the X–X (3, −1) critical point (CP) characteristics in the LAP carboxyl and ammonium groups with those of L-alanine and L-dopa. Very good concordance is observed in the ρ_{CP} and $\nabla^2\rho_{CP}$ values, except for $\nabla^2\rho_{CP}$(C—O) in LAP. However, whereas ε_{CP}(C—O) values are in reasonable agreement, the ε_{CP}(C—N) values are very

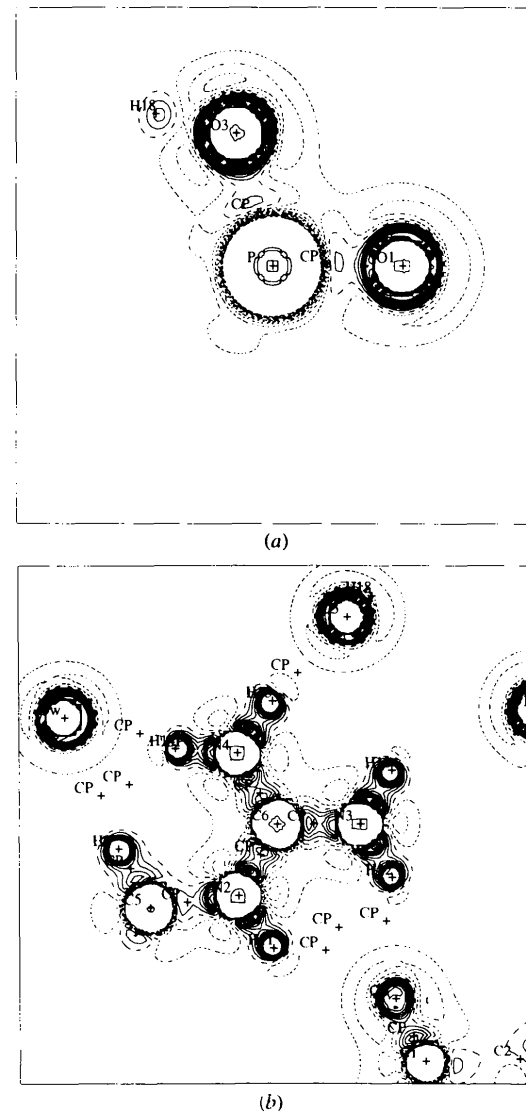

Fig. 8. Negative Laplacian of the electron density and critical points (CP's) from the X–($X + N$) model in (*a*) O1—P—O3 and (*b*) N3—C6—N4 planes. Contour intervals are at 5 e Å^{-5}; dotted lines positive, solid lines negative and zero contour as broken lines. The CP positions are marked by '+'.

*See deposition footnote on p. 525.

Table 11. *X–X topological characterization of the $H_3N—CH—COO$ experimental electron density group in* L*-dopa,* L*-alanine and LAP*

Electron density (ρ), Laplacian ($\nabla^2\rho$), ellipticity (ε) and distance from CP to atom a (d_a) values are referred at each (3,−1) CP. Units are as in Table 10.

Compound	$a—b$ bond	d_a	d_b	ρ	$\nabla^2\rho$	ε
L-dopa	C—N	-	0.591	1.62	−8.4	0.47
	C—O	-	0.614	2.84	−38.8	0.25
		-	0.649	2.70	−32.6	0.25
	$C_N—C_O$	-	0.508	1.71	−12.0	0.14
	C—H	0.653	~0.407	1.98	−19.6	0.13
	N—H	0.740	~0.270	2.38	−28.0	0.02
		0.753	~0.257	1.96	−21.0	0.06
		0.773	~0.237	2.10	−30.0	0.02
L-alanine	C—N	0.635	~0.853	1.70	−11.0	0.30
	C—O	0.540	~0.727	2.86	−29.5	0.13
		0.517	~0.731	3.02	−39.0	0.19
	$C_N—C_O$	~0.756	0.779	1.76	−10.9	0.21
	C—H*	0.758	~0.345	1.66	−11.0	0.09
	N—H†	0.800	~0.248	1.80	−13.2	0.02
LAP	C—N	0.655	0.835	1.70	−8.3	0.08
	C—O	0.494	0.751	2.68	−23.7	0.20
		0.514	0.755	2.59	−23.7	0.20
	$C_N—C_O$	0.748	0.787	1.60	−11.6	0.20
	C—H	0.785	0.301	1.71	−16.9	0.04
	N—H	0.816	0.216	1.97	−35.2	0.02
		0.798	0.234	1.96	−31.3	0.03
		0.816	0.216	1.81	−28.0	0.01

* Average values for the four C—H bonds. † Average values for the three N—H bonds. All approximate values (~) are calculated from the differences between the $a—b$ bond distance and d_a or d_b.

different. A reasonable agreement also exists in the topological features involving H atoms in spite of the different refinement strategies and models, except for the $\nabla^2\rho_{CP}$(N—H) and $\nabla^2\rho_{CP}$(C—H) values in L-alanine.

The C···N and C=O bond critical point characteristics calculated by Souhassou (1995) in biotin-like molecules are also in excellent agreement with those found in this paper: in the C=N bonds, the density and the Laplacian at the critical point range, respectively, from 2.32 to 1.82 e Å^{-3} and from −20.0 to −9.4 e Å^{-5} in Souhassou's work, compared with values from 2.37 to 1.59 e Å^3 and from −20.7 to −6.6 e Å^{-5} in LAP, in close relation with bond strength. The corresponding ρ_{CP} and $\nabla^2\rho_{CP}$ values for C=O are on average 2.82 e Å^{-3} and −25.0 e Å^{-5} for biotin-like molecules compared with the average values 2.65 e Å^{-3} and −23.7 e Å^{-5} in the *X–X* refinement of LAP.

8. Conclusions

Even if the *X*–(*X* + *N*) model is methodologically superior, reliable electrostatic potential calculations and electron density parameters can be achieved by means of the *X–X* model. In particular, outside the molecular van der Waals surface, the electrostatic potential differences between both models agree almost quantitatively. Therefore, *X–X* refinement is adequate to study electrostatic interactions between molecules, as reactivity and molecular recognition, which behaviours are mainly described by the $V(\mathbf{r})$ function out of the van der Waals surface.

This work has been supported by the PB90-0134 project from Dirección General de Investigación Científica y Téchnica (DGICYT), the University Henri Poincaré, the CNRS (URA 809) and the CNI/MAT community (Calcul Numérique Intensif en Sciences des Matériaux). E. Espinosa thanks the Comissionat per a Universitats i Recerca de la Generalitat de Catalunya for a fellowship. We are very grateful to Drs N. E. Ghermani and M. Souhassou for help in the calculations of electrostatic potential, dipole moment and topology of the electron density. We thank one referee for helpful comments.

References

Allen, F. (1986). *Acta Cryst.* B**42**, 512–522.
Aoki, K., Nagano, K. & Iitaka, Y. (1971). *Acta Cryst.* B**27**, 11–23.
Bader, R. F. W. (1990). Atoms and molecules a quantum theory, *The International Series of Monographs on Chemistry*, edited by J. Halpen & M. L. H. Green. Oxford: Clarendon Press.
Becker, P. J. & Coppens, P. (1974). *Acta Cryst.* A**30**, 129–147.
Blessing, R. H. (1986). *Acta Cryst.* B**42**, 613–621.
Blessing, R. H. (1987). *Crystallogr. Rev.* **1**, 3–58.
Blessing, R. H. (1988). *Acta Cryst.* B**44**, 334–340.
Blessing, R. H. (1989). *J. Appl. Cryst.* **22**, 396–397.
Boukhris, A., Souhassou, M., Lecomte, C. & Kempf, J. Y. (1994). Sagamore XI, Brest, France, 7–12 August. Extended Abstracts, *Abstr.* P4-57, p. 260.
Clementi, E. (1965). *IBM J. Res. Develop.* **9**, Suppl., 11–15.
Coppens, P. (1967). *Science*, **158**, 1577–1579.
Coppens, P. (1982). *Electron Distributions and the Chemical Bond*, edited by P. Coppens & M. B. Hall, pp. 61–92. New York: Plenum Press.
Coppens, P., Dam, J., Harkema, S., Feil, D., Feld, R., Lehmann, M. S., Goddard, R., Kruger, C., Hellner, E., Johansen, H., Larsen, F. K., Koetzle, T. F., McMullan, R. K., Maslen, E. N. & Stevens, E. D. (1984). *Acta Cryst.* A**40**, 184–195.
Coppens, P., Guru Row, T. N., Leung, P., Stevens, E. D., Becker, P. J. & Yang, Y. W. (1979). *Acta Cryst.* A**35**, 63–72.
Cromer, D. T. (1974). *International Tables for X-ray Crystallography*, edited by J. Ibers & W. E. Hamilton, pp. 148–151. Birmingham: Kynoch Press.
Cruickshank, D. W. J. (1949). *Acta Cryst.* **2**, 65–82.
Destro, R., Bianchi, R., Gatti, C. & Merati, F. (1991). *Chem. Phys. Lett.* **186**, 47–52.
Dhanaraj, G., Srinivasan, M. R. & Bhat, H. L. (1991). *J. Raman Spectrosc.* **22**, 177–181.
Dhanaraj, G., Srinivasan, M. R., Bhat, H. L., Jayanna, H. S. & Subramanyam, S. V. (1992). *J. Appl. Phys.* **72**, 3464–3467.
Eimerl, D., Velsko, S. P., Davis, L., Wang, F., Loiacono, G. & Kennedy, G. (1989). *IEEE. J. Quantum Electron.* **QE-25**, 179–193.
Epstein, J., Ruble, J. R. & Craven, B. M. (1982). *Acta Cryst.* B**38**, 140–149.

Espinosa, E. (1994). PhD thesis, University of Barcelona, Spain.

Espinosa, E., Molins, E., Veintemillas, S. & Miravitlles, C. (1995). *Z. Kristallogr.* **210**, 195–198.

Espinosa, E., Wyncke, B., Bréhat, F., Veintemillas, S., Molins, E. & Lecomte, C. (1994). *Inf. Phys. Technol.* **35**(4), 625–632.

Fuchs, B. A., Syn, C. K. & Velsko, S. P. (1989). *Appl. Opt.* **28**, 4465–4472.

Ghermani, N., Bouhmaida, N. & Lecomte, C. (1992). *ELECTROS. Computer Program to Calculate Electrostatic Properties from High Resolution X-ray Diffraction.* Internal Report URA CNRS 809, University of Nancy 1, France.

Hansen, N. K. & Coppens, P. (1978). *Acta Cryst.* A**34**, 909–921.

Hanson, J. C., Sieker, L. C. & Jensen, L. H. (1973). *Acta Cryst.* B**29**, 797–808.

Hirshfeld, F. L. (1976). *Acta Cryst.* A**32**, 239–244.

Howard, S. T., Hursthouse, M. B., Lehmann, C. W. & Poyner, E. A. (1995). *Acta Cryst.* B**51**, 328–337.

Johnson, C. K. (1976). *ORTEP*II. Report ORNL-5138. Oak Ridge National Laboratory, Tennessee, USA.

Kitaoka, Y., Yokotani, A. & Sasaki, T. (1989). *Technol. Rep. Osaka Univ.* **39**, 173–179.

Kvick, A., Koetzle, T. F. & Thomas, J. (1974). *J. Chem. Phys.* **61**, 2711–2717.

Moss, G. R. (1983). *MOLDEN and MOLSF. Programs for Calculating Electron Densities and X-ray Structure Factors from a HONDOW Wavefunction.* Buffalo, New York: Hauptman Woodward Institute.

Moss, G. R. & Blessing, R. H. (1984). *Acta Cryst.* A**40**, C-157.

Moss, G. R., Souhassou, M., Espinosa, E., Lecomte, C. & Blessing, R. H. (1995). *Acta Cryst.* B**51**, 650–660.

Saenger, W. & Wagner, K. G. (1972). *Acta Cryst.* B**28**, 2237–2244.

Sasaki, T., Yokotani, A., Fujioka, K., Yamanaka, T. & Nakai, S. (1989). *Technol. Rep. Osaka Univ.* **39**, 25–32.

Sears, V. F. (1992). *Neutron News*, **3**(3), 26–37.

Souhassou, M. (1992). *Am. Crystallogr. Assoc. Meet.* Pittsburgh, Pennsylvania, August. *Abstr.* FO6.

Souhassou, M. (1995). Personal communication.

Souhassou, M., Espinosa, E., Lecomte, C. & Blessing, R. H. (1995). *Acta Cryst.* B**51**, 661–668.

Spackman, M. A. (1992). *Chem. Rev.* **92**, 1769–1797.

Stewart, R. F. & Spackman, M. A. (1983). *VALRAY User's Manual.* Carnegie-Mellon University, Pittsburgh, USA.

Stewart, R. F., Davidson, E. R. & Simpson, W. T. (1965). *J. Chem. Phys.* **43**, 175–187.

Tenzer, L., Frazer, B. C. & Pepinsky, R. (1958). *Acta Cryst.* **11**, 505–509.

Thornley, F. R. & Nelmes, R. J. (1974). *Acta Cryst.* A**30**, 748–757.

Wiest, R., Pichon-Pesme, V., Bénard, M. & Lecomte, C. (1994). *J. Phys. Chem.* **98**, 1351–1362.

Xu, D., Tiang, M. & Tan, Z. (1983). *Acta Chim. Sin.* **2**, 230–233.

Yokotani, A., Sasaki, T., Yoshuda, K. & Nakai, S. (1989). *Appl. Phys. Lett.* 55, 2692–2693.